RESEARCH ARTICLE OPEN ACCESS

Neurodegeneration and Demyelination in the Multiple Sclerosis Spinal Cord

Clinical, Pathological, and 7T MRI Perspectives

Kedar R. Mahajan,[1,2] Danielle Herman,[2] Yufan Zheng,[3] Caroline Androjna,[3] Bhaskar Thoomukuntla,[3] Daniel Ontaneda,[1] Kunio Nakamura,[3] and Bruce D. Trapp[2]

Correspondence
Dr. Mahajan
mahajak@ccf.org

Neurology® 2025;104:e210259. doi:10.1212/WNL.0000000000210259

Abstract

Background and Objectives

Key findings in people with multiple sclerosis (MS) with progressive motor disability are spinal cord (SC) atrophy signifying irreversible axonal loss and SC demyelinated lesions. This study aimed to identify neurodegenerative changes and assess the clinical impact and pathologic characteristics of SC lesions.

Methods

A cross-sectional study was performed using postmortem cervical cord segments from the Cleveland Clinic MS Rapid Autopsy Program. Inclusion included proximity to our center, absence of transmissible infections, and lack of prolonged hypoxia. In situ MRIs were performed before tissue removal and fixation followed by 7T MRI and immunohistochemistry. Quantitative T2* relaxation times were correlated with myelin, axons, and activated microglia/macrophages (major histocompatibility complex II [MHCII]) using Tukey comparison of means and a linear mixed-effects model; T2* was correlated with clinical disease characteristics using Wilcoxon rank sum.

Results

The study included 40 MS cases (median age 58, female 55%) and 9 controls (median age 69, female 89%). A T2* threshold reliably discriminated demyelination (accuracy 89.7%, sensitivity 95.5%, and specificity 87.0%). Myelin content (95% CI −0.82 to −0.58, estimate −0.70) was the only significant predictor of T2*. T2* hyperintensities within the segments ranged from 0% to 100% (median 33.6, interquartile range 12.9–64.3) with only 57.1% demyelinated. T2*-hyperintense/myelinated regions had increased T2* relaxation time (19.2 ms, 95% CI 9.97–28.4), reduced myelin content (−8.3%, 95% CI −12.1 to −4.4), increased MHCII (3.6%, 95% CI 0.45–6.7), reduced axonal counts (−349.8, 95% CI −565.4 to −134.1), and increased axonal area (2.0 μm^2, 95% CI 1.0–3.1) compared with normal-appearing MRI regions. These regions occurred adjacent to T2*-hyperintense/demyelinated lesions (periplaque) or along tracts (tract-based). 7T postmortem T2* hyperintensities were subtle on clinical 1.5T axial T2, and only 43% were detected sagittally. T2*-hyperintense/demyelinated lesions correlated with Expanded Disability Status Scale (EDSS) (rho = 0.61, $p < 0.0001$) and upper cervical cord area (rho = −0.64, $p < 0.0001$) while T2*-hyperintense/myelinated regions did not.

Discussion

Thresholding 7T T2* postmortem MRI can effectively discriminate demyelinated lesions which correlate with clinical disability and cord atrophy. T2*-hyperintense/myelinated regions exhibit myelin and axonal pathology in periplaque or tract-based distributions suggestive of neurodegeneration. Limitations include sampling of 2-cm of SC across participants making conclusions about proximal and distal pathology difficult.

[1]Mellen Center for MS Treatment and Research, Neurological Institute, Cleveland Clinic, OH; [2]Department of Neurosciences, Lerner Research Institute, Cleveland Clinic, OH; and [3]Department of Biomedical Engineering, Lerner Research Institute, Cleveland Clinic, OH.

The Article Processing Charge was funded by the Cleveland Clinic.

Glossary

DAB = diaminobenzidine; **EDSS** = Expanded Disability Status Scale; **FA** = flip angle; **GM** = gray matter; **IHC** = immunohistochemistry; **IQR** = interquartile range; **MHCII** = major histocompatibility complex II; **MS** = multiple sclerosis; **NAWM** = normal-appearing white matter; **PLP** = proteolipid protein; **ROC** = receiver operating characteristic; **ROI** = regions of interest; **SC** = spinal cord; **TE** = echo time; **TR** = repetition time; **UCCA** = upper cervical cord area; **WM** = white matter.

Introduction

Although highly efficacious disease modifying therapies in multiple sclerosis (MS) can prevent clinical relapses/inflammatory disease activity, most disability accumulation occurs independent of relapses.[1,2] Spinal cord (SC) involvement is a predictor for patients at risk for or those who have already developed a progressive disease course and contributes to lower extremity impairment, bladder/bowel dysfunction, sexual dysfunction, and altered sensation.[3,4] These manifestations often appear insidiously in progressive disease, without a defined relapse or detectable interval change on clinical MRIs.

Studies investigating MRI-based detection of SC MRI T2 hyperintensities and atrophy point to the significant contribution of these factors to clinical disability.[3-6] Some individuals have asymptomatic SC involvement or experience near-complete recovery after a SC clinical relapse. Others experience a progressive decline culminating with severe disability, even from a solitary lesion, particularly when involving the lateral corticospinal tract.[7-9]

SC atrophy is more strongly associated with clinical disability than T2 hyperintensities alone and is predictive of a progressive disease course.[10,11] Focal atrophy at the site of lateral cord hyperintensities (termed "critical") is more common in progressive MS and is associated with unilateral motor progression, likely because of loss of corticospinal tract axons.[3,12]

Some limitations with clinical SC imaging include greater distance from the tissue to the coil (including bone/fat), motion artifact, field-strength, and resolution. Improvements have included long axial coverage of the SC to increase detection of T2-hyperintensities by 150% and 3D gradient echo.[13-15] While current imaging consensus recommendations do not favor 3T over 1.5T for MS diagnosis, 7T detects 52% more white matter (WM) cord hyperintensities per case than 3T because of reduced partial volume effects and improved contrast-to-noise ratio.[16-18] High-field MRI (4.7T/7T) with high image resolution in excised postmortem SC segments have identified areas with variable T2 or proton density signal intensity (intermediate or high) correlating with myelin density and characterized as partially or totally demyelinated.[19-23] Axonal content shows weaker MRI correlation than myelin density, likely due to reduced axonal density in both normal-appearing and demyelinated regions compared with controls.[20,24-26]

Owing to the late appearance of cord atrophy after axonal loss, and limitations with clinical imaging, we aimed to better characterize SC MRI pathology to identify neurodegenerative changes. We hypothesized combining 7T MRI with immunohistochemistry (IHC) would detect heterogeneous cord pathology not apparent with clinical in vivo imaging or with pathologic analysis alone. Our objectives were to evaluate the (1) effectiveness of 7T MRI in discriminating heterogeneity of SC pathology characterized by IHC, (2) relationship of distinct SC hyperintensities with clinical disease characteristics, and (3) differences between clinical and postmortem SC MRIs scans.

Methods

Postmortem Program

SC tissue was obtained from the Cleveland Clinic MS Rapid Autopsy Program.[27] Inclusion criteria include a diagnosis of MS, proximity within 75 miles of the center, and ability to obtain a postmortem MRI within 6 hours of death. Exclusion criteria include prolonged hypoxia or greater than 72 hours of mechanical ventilation, recent CNS infection, HIV, or hepatitis B/C. After a postmortem in situ MRI, the brain and SC are removed and fixed. The MS brain/SC donation program is approved by the Cleveland Clinic Institutional Review Board, and informed consent was obtained either from patients before their death or by their next of kin after death.[27] Electronic medical records for cases used in the study were reviewed to abstract demographic information and clinical disease characteristics including disability, disease course, and disease modifying treatment history. eFigure 1 in the Supplement provides an overview of the number of MS cases used for MRI and immunohistochemistry in the study.

Nine controls without MS or known SC pathology were also used to characterize axonal and microglial/macrophage pathology; details in the Supplement.

Postmortem in Situ MRI Acquisition and Analysis

Postmortem in situ brain imaging was performed on 1.5 or 3-tesla (T) MRI with T1-weighted 3D Magnetization Prepared Rapid Acquisition of Gradient Echo, T2-weighted image, fluid-attenuated inversion recovery, and paired proton density-weighted images with and without magnetization transfer pulse.[27] Volumes of T1 hypointensities and T2 hyperintensities were calculated using a semiautomated technique as previously described.[28] Volumetric measures of brain structures were completed after filling T1 hypointensities. Brain parenchymal, gray matter (GM) WM

fractions were obtained using Statistical Parametric Mapping.[29] Upper cervical cord area (UCCA) was measured with in-house atlas-based segmentation. Cases with poor image quality (e.g., temperature effects) or coverage (upper cervical cord) were excluded from analysis; number of cases for each measure are provided in Table.

Postmortem in situ cervical spine imaging was performed in 11 cases on a 3T Siemens Prisma with axial T2*-Multiple Echo Data Image Combination (T2*-MEDIC) (T2*; 0.35 × 0.35 × 1.5 mm, echo time [TE] 8.6 ms, repetition time [TR] 1240 ms, flip angle [FA] 30°, averages 2), sagittal T2-weighted (0.6 × 0.6 × 3.3 mm, TE 83 ms, TR 4000 ms, FA 160°, averages 2).

Table Demographics, MS Clinical Disease Characteristics, and MRI Measures

Demographics and disease characteristics, n = 40	
Age, median (IQR)	58.0 (19.8)
Female sex (%)	22 (55.0)
Race/ethnicity (%)	
White, non-Hispanic	35 (90.0)
White, Hispanic	1 (2.5)
Black	4 (10.0)
EDSS, median (IQR)	7.0 (1.6)
Disease duration, median (IQR)	19.5 (18.5)
Disease course (%)	
Secondary progressive	28 (70.0)
Primary progressive	7 (17.5)
Relapsing remitting	5 (12.5)
Disease-modifying therapy (within 3 y of death) (%)	
None	18 (45)
Interferon beta	1a/1b 8 (20)
Unknown	5 (12.5)
Methotrexate	4 (10)
Glatiramer acetate	2 (5)
Dimethylfumarate	1 (2.5)
Natalizumab	1 (2.5)
Ocrelizumab	1 (2.5)
Postmortem in situ measures from brain MRI	Median (IQR)
Brain parenchymal fraction, n = 36	0.79 (0.10)
T2-hyperintensity volume (cm^3), n = 36	55.5 (62.7)
T1-hypointensity volume (cm^3), n = 36	19.7 (18.6)
T2T1MTR volume (cm^3), n = 32	14.4 (11.8)
Upper cervical cord area (mm^2), n = 35	70.8 (19.7)

Abbreviations: EDSS = Expanded Disability Status Scale; IQR = interquartile range; MS = multiple sclerosis; MTR = magnetization transfer ratio; T2T1MTR = hyperintense on T2, hypointense on T1, low on magnetization transfer ratio (MTR).

SC Segment Selection and Postmortem Ex Vivo 7T Imaging

SCs were removed as previously described[27]; gross examination was conducted to document the location of the cervical enlargement. Alternate 2 cm segments were fixed in 4% paraformaldehyde in scintillation vials or flash-frozen at the time of autopsy. The following day, the specimens were placed into fresh 4% paraformaldehyde. Three days after autopsy, the specimens were rinsed in 0.4M Sorenson's phosphate buffer and placed in cryoprotection solution (20% glycerol, 80mM Sorenson's buffer, and 0.02% sodium azide in MilliQ water). The cervicothoracic junction was an identifiable landmark to select a fixed segment rostrally for MRI-pathology correlations. A custom 3D-printed holder retained each specimen while imaging in a Bruker Biospec 7T scanner with a 23 mm coil. Sequences included T2*-weighted multiple gradient echo (T2*); 0.100 × 0.100 × 0.800 mm, TE = 4.8 ms, echo spacing 5 ms, 8 echoes, TR 2225 ms, FA 50, averages 2, acquisition time 14 minutes, up to 32 slices acquired, and T2-Turbo-Rapid Acquisition with Relaxation Enhancement (T2; 0.100 × 0.100 × 0.800 mm, TE 33 ms, TR 3370 ms, averages 6, acquisition 10 minutes). T2* hyperintensities in each of the ~ 2 cm lower cervical cord SC segments were manually segmented by 2 raters by consensus to obtain the mean cord area, cord volume, T2*-hyperintensity volume, and WM fraction.

Seven cases had 1.5T cervical SC MRI acquired clinically before death.

T2* of non-MS controls could not be compared with MS because they were imaged using a different 3D printed holder and MRI coil.

Postmortem SC MRI T2*-Hyperintensity Segmentation

FSLView (v3.2.0) was used to label MRI regions of interests (ROIs) on the T2* slice corresponding to the myelin (proteolipid protein [PLP]) stained tissue section: T2* normal-appearing on MRI—myelinated on PLP, T2* hyperintense on MRI—myelinated on PLP, or T2* hyperintense on MRI—demyelinated on PLP.[30] Quantitative T2* values for the regions were derived from the multiple gradient echoes as a monoexponential decay.

Immunohistochemistry of SC Sections

SC was dissected in the region corresponding with T2* hyperintensities and cut using a sliding microtome to 30-μm thick sections. Segments without T2* hyperintensities had ~ 0.5 cm of either end removed for sectioning and characterization. IHC techniques for 3,3'-diaminobenzidine (DAB) staining of 30 μm free-floating sections were as described previously and included eMethods in the Supplement.[31]

Based on myelin staining, ROIs were identified in normal-appearing and demyelinated WM/GM; additional ROIs in myelinated areas that were T2* hyperintense were added after reviewing both myelin and MRI images conjunctively: (1) normal-appearing—myelinated (normal-appearing white matter [NAWM]/normal-appearing GM), (2) T2*-hyperintense/myelinated (termed "intermediate"), and (3) T2*-hyperintense/demyelinated. Each ROI was imaged at 20X in DAB-stained sections to quantify percent area occupied by myelin, axons, and microglia/macrophages. To quantify axonal size and counts, 3 images per ROI were captured at 40X in DAB sections; 110 locations-regions (e.g., ventral, dorsal, and lateral locations/NAWM, intermediate, demyelinated regions) across 28 MS cases were suitable for analysis. Three images at 40X were also analyzed in the same region of 9 control cases as MS (ventral). Cases were excluded if axons were cut obliquely in the plane of sectioning, tissue was torn, or staining artifacts existed rendering images unsuitable for analysis. Images were analyzed using a custom script using NIH Fiji.[32]

Confocal microscopy was conducted on SC segments with a Zeiss confocal laser scanning microscope 800 at 63X (1.4 aperture) with secondary antibodies Alexa-Fluor goat anti-mouse 488 A11029 and goat anti-rat 594 A11007 (Life Technologies Corporation, Eugene, OR) from 4 cases that contained all 3 ROIs (NAWM, intermediate, demyelinated) on the same section. A Z-stack of three 63X fields were imaged per ROI; representative images shown.

To evaluate the association of microglia with myelinated axons within an intermediate region, a SC segment with an identified intermediate region was sectioned longitudinally, stained for myelin and microglia/macrophages, and imaged using confocal microscopy.

Statistical Methods

Statistical analysis was performed using R Statistical Software (RStudio 2024.09.0 + 375/R 4.4.1).[33] Tukey honestly significant difference for multiple comparisons of means was used to compare normal-appearing, intermediate, and demyelinated regions within MS WM and GM independently for T2*, percent occupied by PLP, SMI312, major histocompatibility complex II (MHCII), axonal size and counts. A linear mixed effects model was used to describe T2* with PLP, SMI312, and MHCII as fixed effects and the case as a random effect. As the postmortem cohort was overall older with greater disability, the Wilcoxon rank-sum test was used to evaluate differences in disease characteristics and MRI brain measures with extremes in the percentage of cord segment containing MRI hyperintensities, age, and EDSS. Wilcoxon rank sum was also used to (1) compare axonal measures between the same anatomical location across regions (e.g., ventral intermediate vs ventral NAWM); (2) percent area occupied by microglia between MS and control; and (3) axonal measures between MS and control; data in eAppendix 1 in the Supplement.

Data Availability

Deidentified data that support the findings of this study are available from the corresponding author on reasonable request by qualified researchers whose proposal of data use has been approved by an independent review committee after publication of this article and up to 4 years after publication. Datasets include demographics, clinical disease characteristics, immunohistochemistry, MRI measures, and statistical code used for analysis.

Results

Demographics, Disease Characteristics, and in Situ MRI Measures

Demographics, disability measured by EDSS, MS disease course before death, disease-modifying therapies used within 3 years of death, and in situ brain MRIs were obtained immediately after death for the 40 cases used for MRI-pathology correlations (Table). The cohort median age was 58 years, White non-Hispanic (90%), female (55%), with a long disease duration (median 19.5 years), progressive disease course (87.5%), and severe disability requiring a wheelchair (median EDSS 7.0). Most cases were either on low efficacy (35%) or no treatment (45%) within 3 years of death.

Overview and Comparison of Lesions Between 1.5T Clinical, 3T Postmortem in Situ, and 7T Ex Vivo MRI

Figure 1 demonstrates an overview of the cervical SC in vivo (Figure 1, A and B), postmortem in situ (Figure 1, C and D), selection of a cervical SC segments for imaging (Figure 1, E and F), 7T postmortem imaging (Figure 1G), and IHC to identify demyelination (Figure 1, J–L). T2* hyperintensities were thresholded after performing receiver operator curve analysis (ROC: Figure 2) corresponding to demyelination; outlined thresholded regions in Figure 1H and 3-dimensional (3D; MRIcroGL 1.2.20220720) rendering in red (Figure 1I).[34] Seven cases who had postmortem 7T fixed SC segment WM T2 hyperintensities also had clinical cervical spine MRIs available. A demyelinated lateral cord lesion (Figure 1J) is faintly apparent on postmortem axial in situ 3T (Figure 1D) and clinical 1.5T (Figure 1B). The T2*-hyperintense/myelinated (intermediate) region on the contralateral side is not. Neither regions are perceptible on sagittal planes (Figure 1, A and C). To identify whether postmortem 7T MRI could identify these regions more conspicuously than clinical imaging, we compared 7T with a clinical 1.5T scan which could have been prone to motion artifact and a 3T postmortem in situ scan. WM hyperintensities identified on postmortem 7T T2* were conspicuous on clinical 1.5T in 3/7 (42.9%) cases on sagittal short tau inversion recovery and 7/7 on axial T2. Altogether, postmortem 7T MRI identified WM T2* hyperintensities, corresponding to demyelination, more conspicuously than clinical 1.5T and postmortem 3T scans, with the lesions being visible on axial but not sagittal planes in most cases.

Figure 1 Overview of In Vivo, In Situ, and Postmortem MRI; Immunohistochemistry; and MRI Analysis

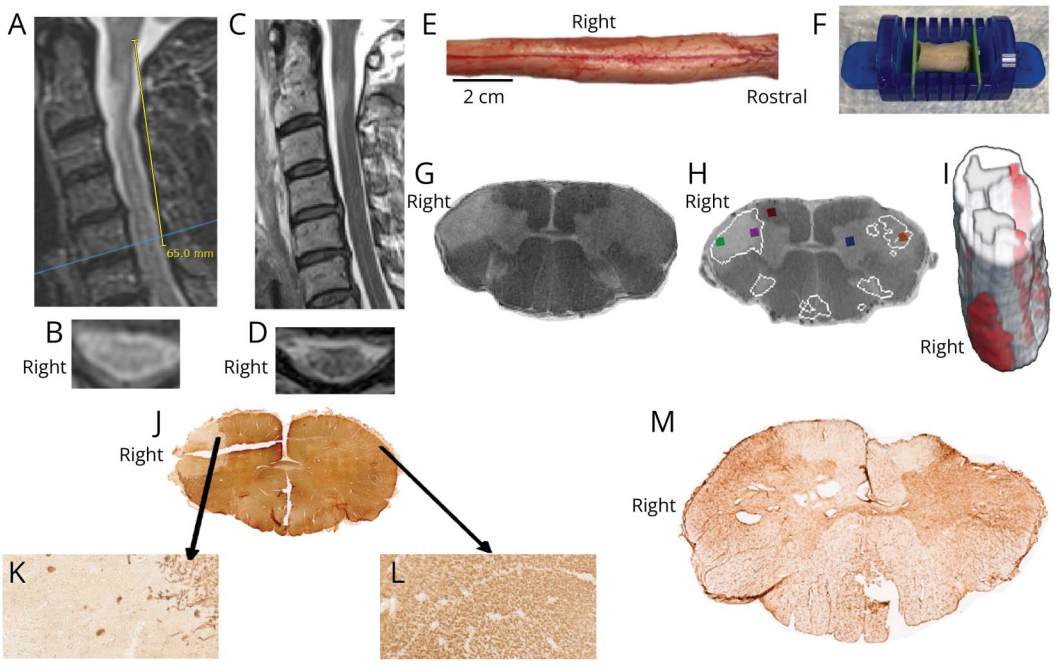

In some cases, a clinical 1.5T (A sagittal, B axial) and postmortem in situ 3T (C, D) cervical spine MRIs were available. Representative autopsy photograph of the postmortem spinal cord with a right lateral cord plaque visible grossly (E; black scale bar 2 cm) with the caudal end of the lesion 6.5 cm distal from cervical level 1 (C1). A fixed cord segment (~2 cm) was selected at the site of the cervical enlargement for postmortem 7T MRI; 3D-printed spinal cord segment holder (F). T2-weighted 7T MRI of a cord segment (G). Based on myelin staining, ROIs were identified in normal-appearing and demyelinated white and gray matter; additional ROIs in myelinated regions that were T2* hyperintense were added after reviewing both myelin and MRI images conjunctively (H). A 3D rendering of T2* hyperintensities above the T2* threshold for demyelination are depicted in red; the right lateral cord lesion is labeled (I). Immunohistochemistry (IHC) using 3',3'-diaminobenzidine (DAB) of myelin (proteolipid protein; PLP, J–L), and activated microglia/macrophages (major histocompatibility complex II), MHCII (M). Demyelinated and myelinated hyperintense regions stained for myelin are shown in (K) and (L), respectively. The right lateral cord lesion is apparent on axial (B, D) but not sagittal T2 (A, C); yellow vertical scale bar in "A" denotes location of right lateral cord lesion observed grossly and with postmortem imaging and IHC. The demyelinated right lateral cord lesion is hyperintense on postmortem 7T MRI (G, H) and is slightly perceptible on in vivo axial 1.5T (B) and postmortem axial in situ 3T (D). The myelinated region in the left lateral cord is T2-hyperintense on postmortem 7T MRI (G, H) but is not visible on axial or sagittal postmortem in situ or clinical cervical spine imaging (A–D). Both myelinated and demyelinated cord regions exhibit increased MHCII (M). IHC = immunohistochemistry; ROC = receiver operating characteristic.

Cervical Cord MRI T2* Hyperintensities Are Variable and Extensive

The percentage of the segment that was T2* hyperintense ranged from 0% to 100% (median 33.6, interquartile range [IQR] 12.9–64.3). eFigure 2 in the Supplement demonstrates variability of hyperintense regions across 2 cases. We observed that while some T2* hyperintensities on MRI corresponded with demyelination (eFigure 2B; red dots), others appeared myelinated or had decreased myelin content compared with normal-appearing WM/GM (eFigure 2B; yellow asterisks). Overall, the extent of T2*-hyperintense regions varied widely across segments, with some regions corresponding to demyelination and others showing preserved or reduced myelin content.

Identifying SC Demyelination Using 7T Postmortem MRI

To determine whether T2* measures can discriminate between a binary classification of myelinated (normal-appearing and intermediate) and demyelinated regions, we performed receiver operating characteristic (ROC) analysis and determined a T2* cutpoint of 47.0 ms above which discriminated WM demyelination with accuracy 89.7%, sensitivity 95.5%, and specificity 87.0% in the WM (Figure 2, A and B left). Similar analysis in the GM was performed with a cutpoint of 44.6 ms, accuracy 84.3%, sensitivity 76.2%, and specificity 90% (Figure 2, A and B right).

SC T2* hyperintensities were automatically segmented using the higher T2* cutpoint of 47.0 ms (for WM demyelination) and correlated with manually segmented T2* hyperintensities (rho = 0.59, p = 0.0008). The percentage of the cord hyperintense above a T2* cutpoint of 47.0 ms was lower (median 9.0%, IQR 28.8%, range 0.19%–82.8%), representing a subset of the total manual hyperintensity mask, by sparing regions that were subtly T2* hyperintense but myelinated (intermediate; eFigure 2B yellow asterisk vs red dots and eFigure 2C).

The WM T2* hyperintensity mask for each cord segment was subclassified by the T2* relaxation time that was above (T2*-hyperintense/demyelinated) or below (T2*-hyperintense/myelinated; intermediate) the cutpoint (47 ms). The distribution of T2*-hyperintensity thresholded as myelinated or demyelinated varied across cases (Figure 2C). Figure 3, A and D, demonstrate a representative cord segment with putative T2*-hyperintense/myelinated (green) and T2*-hyperintense/

Figure 2 Discriminating Spinal Cord MRI Hyperintensities With Pathologic Characterization

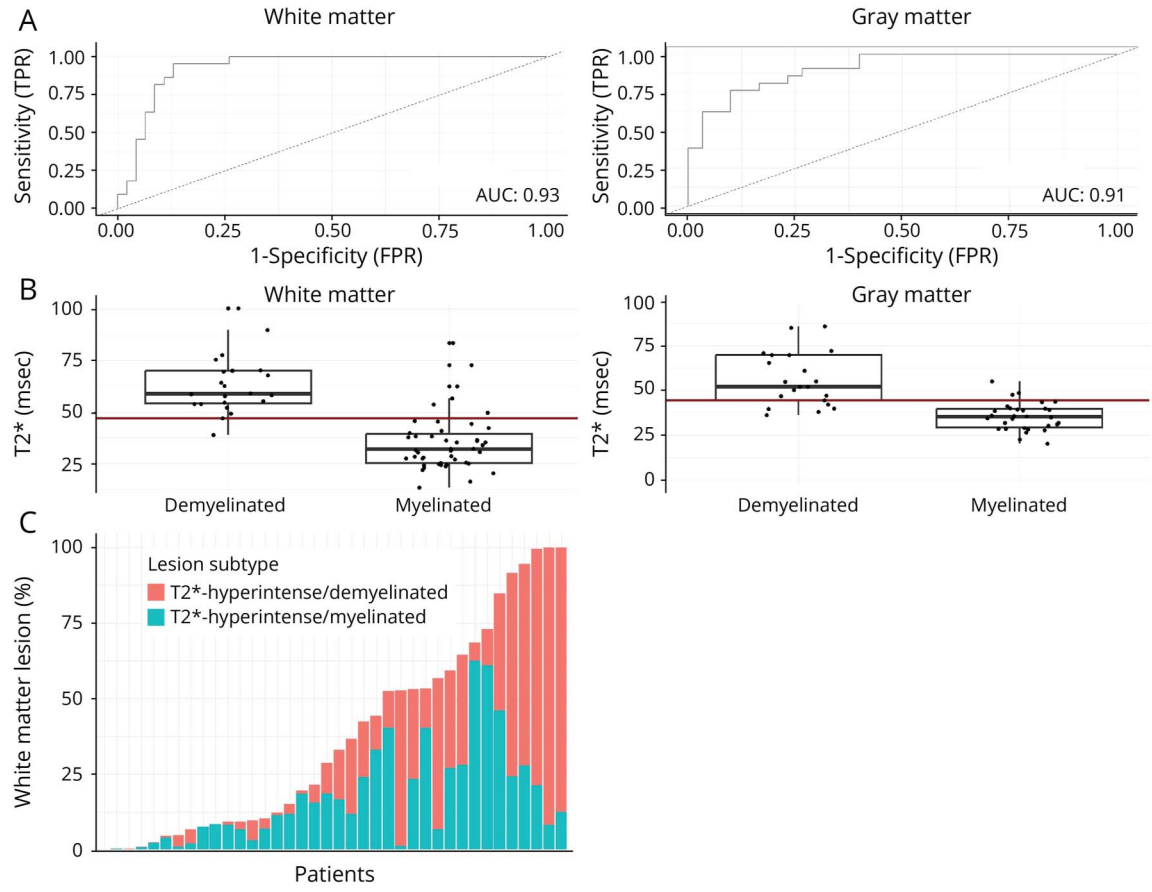

(A) Receiver operating characteristic (ROC) analysis plotting sensitivity (true positive rate [TPR]) vs 1-specificity (false-positive rate [FPR]) for WM and G. (B) The optimal cutpoint from ROC analysis was a T2* of 47.0 ms to discriminate demyelinated lesions vs myelinated regions (including both NAWM and intermediate WM regions) by immunohistochemistry for myelin for WM and 44.6 ms for GM. (C) A T2* threshold was used to subclassify WM T2* hyperintensities into a putative T2*-hyperintensity/myelinated (intermediate) and T2*-hyperintense/demyelinated masks. A stacked and rank-ordered bar plot of the percentage of each cord segment that was T2*-hyperintense in the WM is shown. GM = gray matter; NAWM = normal-appearing white matter; WM = white matter.

demyelinated (red) regions in 3D (Figure 3D).[34] The dorsal cord has a subtle T2*-hyperintensity (intermediate) extending throughout the cord segment, is myelinated (Figure 3, B and F), and has increased microglia/macrophage content relative to NAWM (Figure 3E). The lateral cord hyperintense (red) region is demyelinated (Figure 3, B and C) with increased microglia/macrophages (Figure 3E) in the periplaque WM (blue arrowhead) with reduced myelin density and within the demyelinated GM. T2* measures from 7T postmortem MRI accurately distinguish myelinated and demyelinated SC regions.

7T MRI-Immunohistochemistry Correlates of SC Regions

Initially MRI T2* regions were identified as myelinated or demyelinated based on myelin staining of the respective MRI slice/IHC tissue section. Later, regions noted to be myelinated (by PLP) but appeared abnormal on T2* were classified as T2*-hyperintense/myelinated regions while T2* regions that were demyelinated were classified as T2*-hyperintense/demyelinated. We obtained quantitative T2* in each of these regions along with the percentage of area occupied by myelin, activated microglia/macrophage, and axonal staining (Figure 4, A–D). Demyelinated WM and GM regions expectedly had greater T2* intensity and lower myelin content (Figure 4A). T2*-hyperintense/myelinated regions (intermediate) had T2* and myelin measures between NAWM and demyelinated regions (Figure 4, A and B). Intermediate regions also had more activated microglia/macrophages than normal-appearing and demyelinated regions (Figure 4C). Total area occupied by staining for axons did not vary between the groups; axonal size and counts described below however did vary (Figure 4D). Only myelin content (95% CI −0.82 to −0.58, estimate −0.70) was a significant predictor of T2* when including myelin, activated microglia/macrophage, and axonal measures in a linear mixed effects model; for every 0.70 ms increase in WM T2* relaxation time, the area occupied by PLP decreased by 1%. GM regions followed similar trends. Collectively, T2* intensity was highest in demyelinated regions with myelin content being the strongest predictor of T2* values, while intermediate regions also exhibited increased microglia/macrophage activity.

Figure 3 Periplaque and Tract-Based Distribution of Intermediate Regions

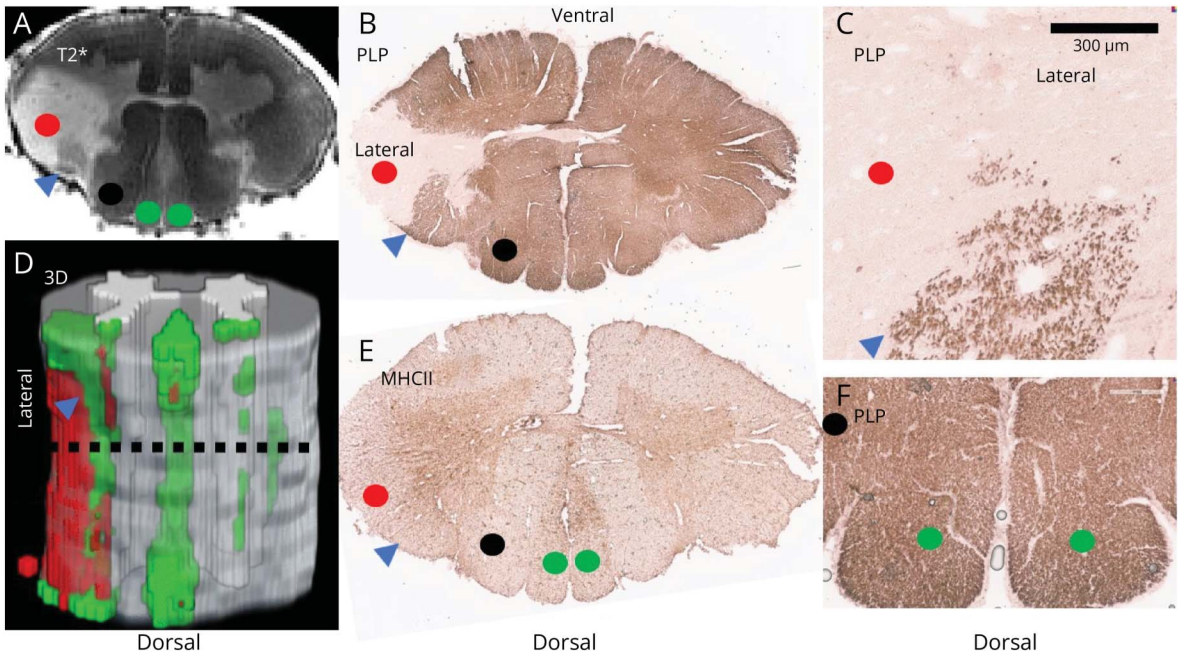

Representative images of MRI and IHC from a cervical spinal cord segment. Putative subtypes of regions are denoted by red (T2*-hyperintense/demyelinated), green (T2*-hyperintense/myelinated, intermediate), and black (NAWM) dots. (A) lateral demyelinated intermediate lesions are evident. (B) Lateral hyperintensity is demyelinated while the dorsal region is myelinated. (C) Myelin is reduced adjacent to the lateral demyelinated lesion at higher magnification (blue arrowhead). (D) 3D rendering of putative T2*-hyperintense myelinated and demyelinated regions along the 2 cm cord segment derived from the T2* threshold; dashed line corresponds to the location of the MRI and IHC slice. Intermediate regions follow the dorsal gracile fasciculus or are adjacent to demyelinated lesion (periplaque; blue arrowhead). (E) The gracile fasciculus and periplaque region have increased microglia/macrophages and is myelinated (F). IHC = immunohistochemistry; MHCII = major histocompatibility complex II (activated microglia/macrophages); NAWM = normal-appearing white matter; PLP = proteolipid protein (myelin).

Axonal Characteristics of T2*-Hyperintense/Myelinated (Intermediate) Regions

Confocal microscopy was performed to visualize whether regions with decreased myelin content had demyelinated axons or other axonal pathology. Figure 5 shows images from NAWM, intermediate WM, and demyelinated WM (left to right, respectively). We observed axons within intermediate regions were myelinated. The inset in Figure 5 demonstrates an intermediate region with a myelinated axon (white arrowhead), mostly demyelinated axon (cyan arrowhead) and a myelin sheath without an axon (yellow arrowhead).

Axonal size and counts (Figure 5) were measured using DAB free-floating sections. Axonal size was increased in intermediate (7.99 ± 2.01 μm^2) and demyelinated (8.24 ± 2.29 μm^2) regions compared with NAWM (5.96 ± 1.31 μm^2); all $p < 0.001$; details across different anatomical SC locations in eTables 1 and 2 in the Supplement.

In aggregate, intermediate regions exhibited signs of neurodegeneration with increased axonal size and reduced axonal counts compared with NAWM.

Clinical and in Situ MRI Brain Correlations of Cord Segment Pathology

Because cord atrophy and T2 hyperintensities have been previously shown to correlate with clinical disability and risk of progression, we evaluated the relationship of SC segment MRI T2* hyperintensity burden, age, EDSS, disease duration, and MRI brain measures.[5,10,12]

The total T2* hyperintensity burden was used to compare the first quartile (0–25th percentile) (lower T2* hyperintensity burden; n = 10; median percentage cord segment with a T2* hyperintensity 4.9% [IQR 6.4%]) and 4th quartile (75th—100th percentile) (higher T2* hyperintensity burden; n = 10; 87.6% [17.6]). Only age (61.0 [IQR 13.3] vs 43.0 [15.5] years; $p = 0.02$) was significantly different. Similarly, the youngest cases (first quartile; age; n = 10) in the cohort (38.5 [5.8] vs 71.0 [6.8] years) had higher cord segment T2* hyperintensity burden (66.2% [34.7] vs 20.7% [26.8]; $p = 0.005$) than the oldest cases (fourth quartile, n = 10).

Cases with the greatest disability [80th–100th percentile, n = 9; EDSS 9.0 (0.5)] had greater T2* hyperintensity burden [85.2% (38.8) vs 16.6% (14.0), $p < 0.001$], brain T2LV (112.3 [42.6] vs 24.8 [16.8] cm^3, $p = 0.008$), T1LV (35.7 [8.6] vs 12.8 [6.7] cm^3, $p = 0.008$), and hyperintense on T2, hypointense on T1, low on magnetization transfer ratio LV (22.6 [24.2] vs 10.7 [6.1] cm^3, $p = 0.01$) compared with those with the least disability (0–20th percentile, n = 9, EDSS 4.0 [3.0]).

We next sought to determine whether the effect of T2* hyperintensity burden on disability and cord atrophy varied

Figure 4 Pathologic Correlates of Intermediate Regions

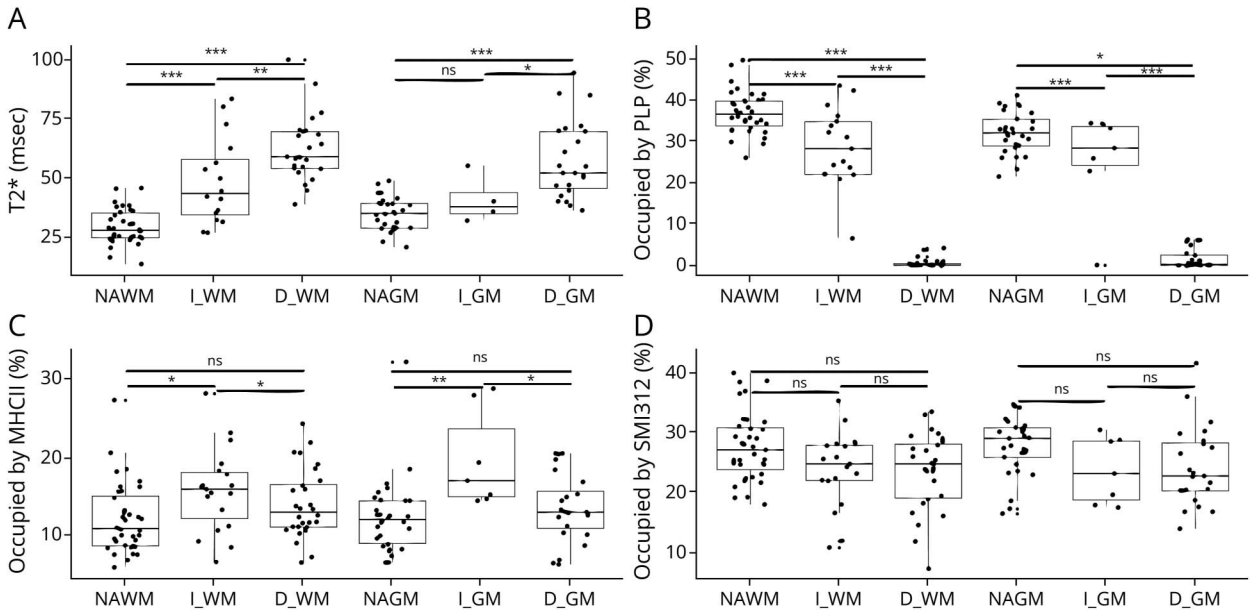

White matter (WM) and gray matter (GM) regions were characterized by (A) T2* measures, (B) myelin (PLP, proteolipid protein), (C) activated microglia/macrophages (MHCII, major histocompatibility complex II), and (D) axons/dendrites (SMI312) in each respective region of interest. Each spinal cord segment varied on the presence of NAWM, intermediate, or demyelinated regions. Tukey HSD was used to compare groups within WM/GM; *$p < 0.05$, **$p < 0.005$, ***$p < 0.0005$, NS—not significant. D_GM = demyelinated GM; D_WM = demyelinated WM; I_GM = intermediate GM; I_WM = intermediate WM; NAGM = normal-appearing GM; NAWM = normal-appearing WM.

based on the T2* intensity based on our T2* threshold for demyelination. EDSS correlated modestly with the total T2* hyperintensity burden within the cord segment (Spearman rho = 0.48, $p = 0.001$) and better with the putative T2*-hyperintense/demyelinated lesion burden (rho = 0.61, $p < 0.0001$); intermediate regions did not correlate (rho = 0.24, $p = 0.14$). Similarly, UCCA obtained from the postmortem in situ MRI brain correlated modestly with total T2*-hyperintensity burden within the cord segment (rho = −0.46, $p = 0.006$) but best with the putative T2*-hyperintense/demyelinated lesion burden (rho = −0.64, $p < 0.0001$); the intermediate regions did not correlate (rho = −0.19, $p = 0.28$).

Because individuals with MS can have lesions present in the brain and SC proportionately or disproportionately, we evaluated whether distinct SC T2* hyperintensities correlate with in situ MRI brain measures. We found T2*-hyperintense/demyelinated SC volume weakly correlated with in situ brain T2-lesion volume (rho = 0.39, $p = 0.03$), but T2*-hyperintense/myelinated volumes did not (rho = −0.07, $p = 0.70$). Neither T2*-hyperintense/myelinated or T2*-hyperintense/demyelinated SC lesion volumes correlated with in situ MRI brain T1-lesion volume (rho = −0.02, $p = 0.92$; rho = 0.29, $p = 0.09$, respectively) or brain parenchymal fraction (rho = −0.009, $p = 0.96$; rho = −0.20, $p = 0.27$).

Taken together, T2*-hyperintense/demyelinated lesion burden correlated more strongly with clinical disability, cord atrophy, and brain T2-lesion volume than T2*-hyperintense/myelinated regions, highlighting the clinical relevance of discriminating demyelinated lesions.

MS SC T2*-Hyperintense Regions Have Variable Microglia/Macrophage Activity

Although increased activated microglia/macrophages (MHCII) were seen in some demyelinated lesion centers (Figure 6A) and borders (Figure 6B), their expression varied. Figure 6C shows a dorsal demyelinated lesion with decreased MHCII while Figure 6D demonstrates a region with decreased myelin content. Sections from the 40 cases were characterized based on MHCII and PLP staining, and 112 T2* hyperintense were identified (Figure 6). Most regions were classified as intermediate (34/112; 30.4%), followed by demyelinated lesions with increased MHCII (27/112, 24.1%), greater MHCII at the lesion border (19/112, 17.0%), and decreased MHCII expression (18/112, 16.1%). Some demyelinated lesions had similar MHCII density compared with normal-appearing regions (14/112, 12.5%). Distally to an intermediate region, microglia appeared in association with myelin sheaths (Figure 6E). The diverse patterns of activated microglial/macrophage observed here underscore their potential for distinct functions within intermediate or demyelinated regions.

Discussion

SC involvement in MS particularly leads to disability given the presence of critical motor and sensory pathways. Here we

Figure 5 Decreased Axonal Density and Increased Axonal Size Within Spinal Cord Intermediate WM Regions

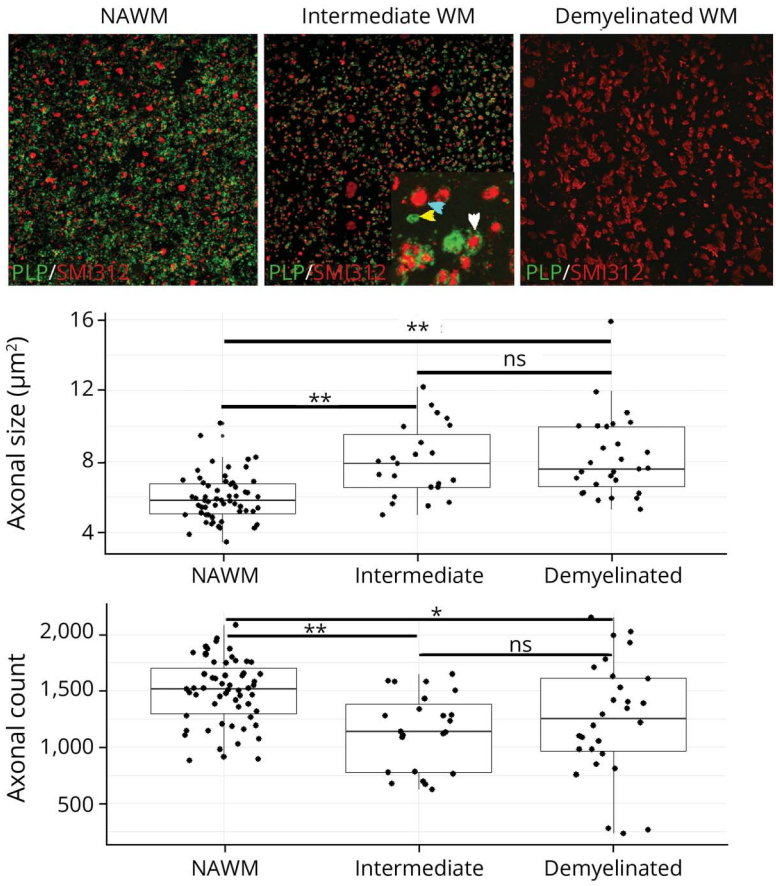

Confocal microscopy was performed on 4 cases with all 3 regions of interest. Representative confocal images of T2*-isointense/myelinated (NAWM), T2*-hyperintense/myelinated WM (Intermediate; enlarged inset shown), and T2*-hyperintense/demyelinated WM (Demyelinated). Enlarged inset of the intermediate region with a myelinated axon (white arrowhead), enlarged axon with reduced myelin (cyan arrowhead), and a myelin sheath without an axon (yellow arrowhead). Axonal size and counts were obtained from 3,3′-diaminobenzidine (DAB) stained sections from a mean of 3 images taken at ×40 from 110 locations-regions (e.g., lateral, dorsal cuneate fasciculus, dorsal gracile fasciculus, ventral/NAWM, intermediate, demyelinated) across 28 cases. Axonal size in intermediate and demyelinated regions were increased while axonal counts were reduced in intermediate and demyelinated regions relative to NAWM. Significance using Tukey honest significance test; *p < 0.05, **p < 0.005, NS—not significant. NAWM = normal-appearing WM; WM = white matter.

sought to evaluate SC tissue by IHC and correlate findings with 7T to better understand the heterogeneity of SC pathology. T2* was able to discriminate demyelinated SC lesions from T2*-hyperintense/myelinated and normal-appearing regions and demyelinated lesions correlated strongly with EDSS and UCCA; T2*-hyperintense/myelinated regions did not.

Our results concur with findings by Bot et al.[20] 2004 that SC T2*-hyperintense myelinated regions had reduced myelin content but differed because we also detected increased axonal size and reduced axonal counts. The association with MRI intensity and myelin density has also been noted in the marmoset SC with experimental autoimmune encephalomyelitis.[35] Axons within intermediate regions were myelinated but with reduced myelin content overall. We speculated that tracts within intermediate regions are undergoing neurodegeneration, possibly because of demyelinating lesions present rostrally/caudally. MS neurodegenerative changes may be akin to anterograde/retrograde changes within the cord seen after severe traumatic SC injury.[36] Our work highlights dorsal WM tracts may particularly be susceptible to neurodegeneration. Watershed territories supplied by non-anastomosing end arteries may be more prone to demyelination such as the periventricular WM lying between the anterior/middle cerebral arteries in both MS and cerebral microvascular disease.[37,38] The lateral SC lying between the anterior/posterior spinal arteries and the midline dorsal cord between the paired posterior spinal arteries are potential sites for a hypoxic environment that may lead to a greater extent of axonal injury after demyelination or impaired repair. Furthermore, a vascular disruption of a blood-SC barrier such as within the posterior median vein may represent another mechanism for the prediction of the dorsal cord to demyelination.

Because nerve roots were not individually dissected and labeled at the time of autopsy to identify SC levels, comparing cord and lesion volumes across cases at the segment level was not feasible. While MRI properties can be influenced by fixation time, SC segments in our biorepository were fixed consistently for 3 days before storage in a cryoprotection buffer limiting differences across cases. T2* can however be influenced by the MRI parameters and coil used, making direct comparisons of a T2* value across different coils and scanners challenging; adjusting T2* lesional/NAWM ratios may address this limitation. We lacked the power to detect a difference between neuroanatomical locations (ventral,

Figure 6 Spinal Cord T2* Hyperintensities Have Variable Microglia/Macrophage Patterns

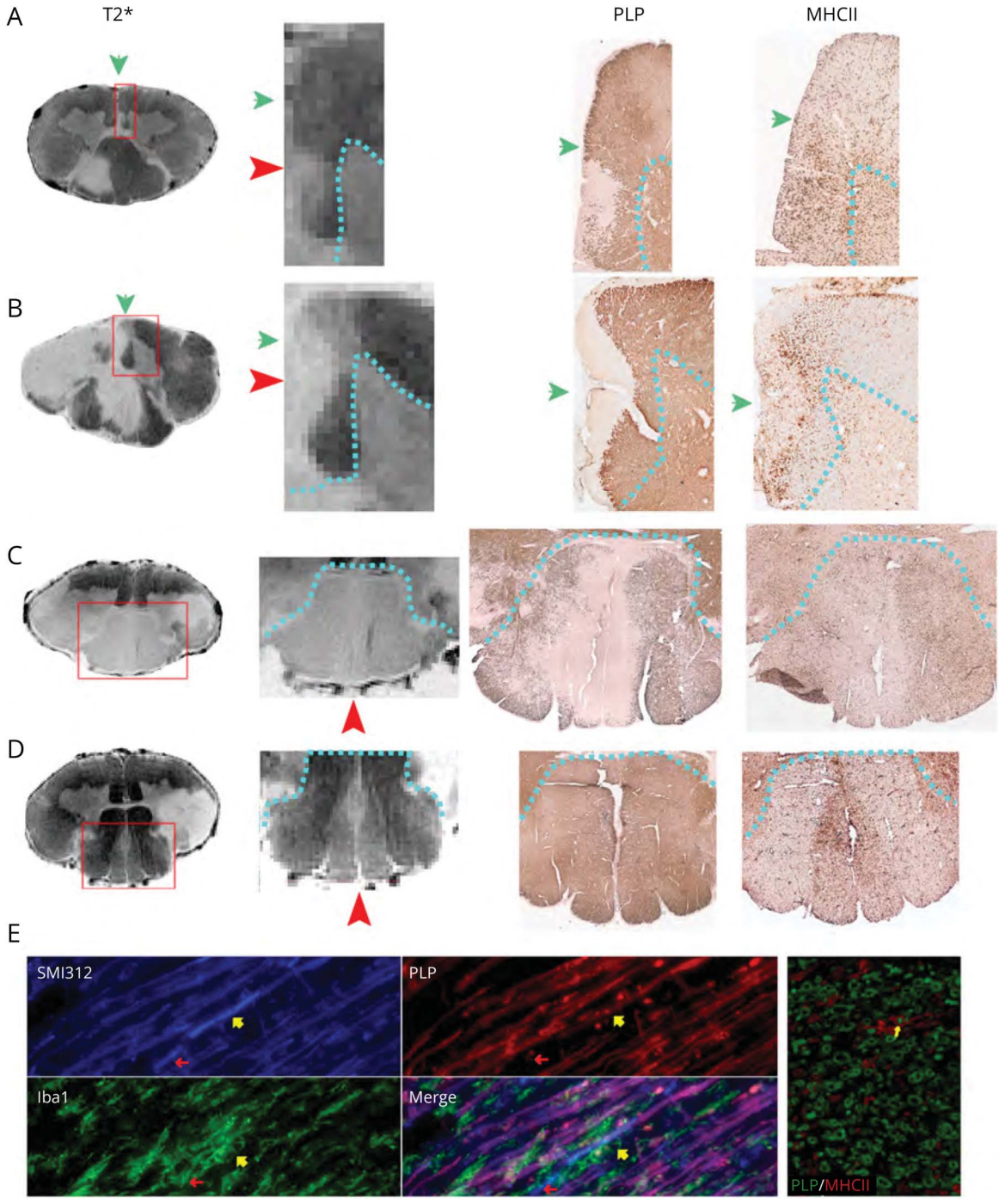

MRI T2* images are shown with the inset (red outline) enlarged. Myelin (PLP) and activated microglia/macrophage (MHCII) immunohistochemistry are shown for the enlarged area. The gray/white matter boundary (dashed cyan line) and the ventral median fissure (green arrow) are shown for orientation. (A) Demyelinated lesion with increased MHCII throughout. (B) Region of demyelination at the subpial cord surface with increased MHCII at the lesion border. (C) Dorsal cord with the gracile fasciculus nearly entirely demyelinated with decreased MHCII; adjacent cuneate fasciculus has reduced myelin with greater MHCII. (D) The dorsal cord with hyperintense gracile fasciculus appearing myelinated with greater MHCII. (E) Microglia appear in close association with myelinated axons in a T2-hyperintense/myelinated region sectioned longitudinally (left) and axially (right). PLP = proteolipid protein.

lateral, and dorsal) for T2*; further studies may need to investigate differences in MRI properties and axonal vulnerability to degeneration because axonal size varies among WM tracts. Some locations such as the unmyelinated substantia gelatinosa inherently has a higher T2* signal and can be inaccurately classified as a demyelinated lesion based on a T2* threshold.

In addition to greater field strength, sequences such as phase sensitive inversion recovery may improve the lesional/

normal-appearing contrast ratio at conventional field strengths.[39] Both focal (Figure 6A) and confluent (Figure 6C) T2* hyperintensities had variable degrees of myelination. We found similar trends with T2* and T2-weighted (Turbo-Rapid Acquisition with Relaxation Enhancement) and T1-weighted (modified driven equilibrium Fourier transform) sequences suggesting these modalities may also be useful improving the specificity for demyelination, particularly as a ratio of lesion/normal-appearing regions. Greater field strength and a multiparametric approach that includes myelin-specific sequences to better identify the extent of myelin and axonal pathology will be important clinically to correlate with clinical disability/outcomes and as an imaging biomarker for neuroprotective and remyelinating therapeutic strategies. Some focal lesions lining the periphery of the cord suggests a CSF mediated mechanism of demyelination rather than perivenular (Figure 6B), perhaps precipitated by dilated SC veins causing reduced glymphatic flow at sites of spinal canal stenosis.[40] The peripheral location of some lesions may also be due to susceptibility of certain peripheral tracts or inflammatory mediators in the CSF-subarachnoid space/meninges.

Overall, our findings highlight the presence of distinct MRI SC lesion subtypes characterized by demyelination and neurodegeneration using 7T MRI of postmortem tissue with pathologic characterization as a benchmark. Clear gaps in detection of lesions from antemortem clinical and postmortem in situ scans are apparent. Improvement of axial SC coverage may be beneficial because some subtle lesions may be missed on sagittal sequences with limited axial coverage. One could postulate that the evaluation of SC for disease activity is particularly imperative if the individual is not on therapy or on low or moderately effective therapies with greater risk for disease activity. As new/enlarging SC T2*-hyperintensities could present with gradual worsening of symptoms rather than a clear clinical relapse, clinicians should be cognizant of potential SC disease activity despite stable brain imaging or SC imaging with inadequate resolution. There is a growing realization of the inclusion of SC monitoring for disease activity rather than solely relying on brain imaging for evaluating disease modifying therapy efficacy.[41-43] Automated tools under development to segment cervical SC GM/WM compartments at 3T may detect regional cord atrophy as an outcome measure for neuroprotective strategies.[44] Remyelinating therapeutic trials could similarly evaluate longitudinal changes in thresholded T2*-hyperintense lesions.

Differences in MHCII expression in demyelinated lesions and intermediate regions (Figure 6) were observed. Reports of iron rim lesions in the cervical cord suggest the few microglia at the border of some demyelinated lesions may be sufficient for MRI susceptibility change.[45,46] Macrophage markers are typically coexpressed in WM lesions compared with GM lesions containing predominantly microglia.[23,47] Regions with decreased myelin relative to NAWM in the SC have been characterized by both proinflammatory and anti-inflammatory markers as well as differential expression of astrocyte genes.[48] This raises the potential that chronic and progressive inflammatory processes in periplaque SC regions contribute to demyelination and remyelination failure.[48]

Future studies can determine whether (1) remyelination or segmental demyelination are contributors to intermediate regions, (2) thresholded T2* hyperintensities in an in vivo cohort differentially predict clinical disability, (3) cases with intermediate areas in the SC also have similar pathology in the cortex and cerebral WM, (4) myelin-specific sequences corroborate with T2* measures, (5) changes in phospholipid content (e.g., Luxol fast blue), correlates with MRI measures independent of myelin content, (6) differential SMI31 (phosphorylated; decreased in MS WM lesions) and SMI32 (non-phosphorylated; increased in damaged axons) expression of axons proximal/distal to demyelinating lesions,[49] and (7) axonal pathology occurs anterograde/retrograde to focal demyelinating lesions in specific tracts.

The detection and characterization of these intermediate regions is a novel opportunity to detect axonal pathology rather than measuring axonal loss by atrophy.[3,5,50] These are requisite steps to identify mechanisms that lead to ongoing myelin and axonal pathology in the MS SC and develop greatly needed neuroprotective and repair strategies.

Author Contributions

K.R. Mahajan: drafting/revision of the manuscript for content, including medical writing for content; major role in the acquisition of data; study concept or design; analysis or interpretation of data. D. Herman: drafting/revision of the manuscript for content, including medical writing for content; major role in the acquisition of data. Y. Zheng: major role in the acquisition of data. C. Androjna: major role in the acquisition of data. B. Thoomukuntla: major role in the acquisition of data D. Ontaneda: drafting/revision of the manuscript for content, including medical writing for content; study concept or design; analysis or interpretation of data. K. Nakamura: drafting/revision of the manuscript for content, including medical writing for content; major role in the acquisition of data; study concept or design; analysis or interpretation of data B.D. Trapp: drafting/revision of the manuscript for content, including medical writing for content; major role in the acquisition of data; study concept or design; analysis or interpretation of data.

Acknowledgment

We thank Dr. Grahame Kidd for helpful discussions on SC confocal microscopy and axonal quantification. The expertise of Mark Howell and Logan Shannon in imaging postmortem SC specimens in the Cleveland Clinic Lerner Research Institute Small Animal Imaging Core facility were greatly appreciated.

Study Funding

This work was supported by funding through the institution from the NIH/NINDS for K.R. Mahajan. (K23NS109328) and B.D. Trapp (R35NS097303).

Disclosure

K.R. Mahajan has received funding by NIH NINDS and has received consultation fees from Genentech/Roche. K. Nakamura has received licensing fees from Biogen Idec, and has received research funding through the institution from NIH, DOD, NMSS, Biogen Idec, Novartis, and Sanofi Genzyme. B.D. Trapp has received grant support from NIH, National Multiple Sclerosis Society, Astoria Biologica; has received speaking fees from Sanofi Genzyme and advisory board fees from Disarm Therapeutics and Cognito; and is a founder of Cashel Neural. The postmortem program is funded by funding from NIH/NINDS R35. D. Ontaneda has received research support from the NIH, the National Multiple Sclerosis Society, the Patient Centered Outcomes Research Institute, the Race to Erase MS Foundation, Genentech, Genzyme, Novartis, and Bristol Myers Squibb; and has received consulting fees from Biogen Idec, Janssen, Genentech/Roche, Genzyme, Novartis, Merck, and Bristol Myers Squibb. D. Herman, Y. Zheng, C. Androjna, and B. Thoomukuntla have nothing to disclose. Go to Neurology.org/N for full disclosures.

Publication History

Received by *Neurology* June 11, 2024. Accepted in final form November 12, 2024. Submitted and externally peer-reviewed. The handling editor was Associate Editor Frederik Barkhof, MD, PhD.

References

1. Kappos L, Wolinsky JS, Giovannoni G, et al. Contribution of relapse-independent progression vs relapse-associated worsening to overall confirmed disability accumulation in typical relapsing multiple sclerosis in a pooled analysis of 2 randomized clinical trials. *JAMA Neurol*. 2020;77(9):1132-1140. doi:10.1001/jamaneurol.2020.1568
2. Kreiter D, Spee R, Merry A, Hupperts R, Gerlach O. Effect of disease-modifying treatment on spinal cord lesion formation in multiple sclerosis: a retrospective observational study. *Mult Scler Relat Disord*. 2023;79:104994. doi:10.1016/j.msard.2023.104994
3. Sechi E, Messina S, Keegan BM, et al. Critical spinal cord lesions associate with secondary progressive motor impairment in long-standing MS: a population-based case-control study. *Mult Scler*. 2021;27(5):667-673. doi:10.1177/1352458520929192
4. Lee LE, Vavasour IM, Dvorak A, et al. Cervical cord myelin abnormality is associated with clinical disability in multiple sclerosis. *Mult Scler*. 2021;27(14):2191-2198. doi:10.1177/13524585211001780
5. Rocca MA, Valsasina P, Meani A, et al. Spinal cord lesions and brain grey matter atrophy independently predict clinical worsening in definite multiple sclerosis: a 5-year, multicentre study. *J Neurol Neurosurg Psychiatry*. 2023;94(1):10-18. doi:10.1136/jnnp-2022-329854
6. Lauerer M, McGinnis J, Bussas M, et al. Prognostic value of spinal cord lesion measures in early relapsing-remitting multiple sclerosis. *J Neurol Neurosurg Psychiatry*. 2023;95(1):37-43. doi:10.1136/jnnp-2023-331799
7. Granella F, Tsantes E, Graziuso S, Bazzurri V, Crisi G, Curti E. Spinal cord lesions are frequently asymptomatic in relapsing-remitting multiple sclerosis: a retrospective MRI survey. *J Neurol*. 2019;266(12):3031-3037. doi:10.1007/s00415-019-09526-3
8. Zecca C, Disanto G, Sormani MP, et al. Relevance of asymptomatic spinal MRI lesions in patients with multiple sclerosis. *Mult Scler*. 2016;22(6):782-791. doi:10.1177/1352458515599246
9. Keegan BM, Kaufmann TJ, Weinshenker BG, et al. Progressive solitary sclerosis: gradual motor impairment from a single CNS demyelinating lesion. *Neurology*. 2016;87(16):1713-1719. doi:10.1212/WNL.0000000000003235
10. Tsagkas C, Huck-Horvath A, Cagol A, et al. Longitudinal assessment of cervical spinal cord compartments in multiple sclerosis. *Mult Scler Relat Disord*. 2023;71:104545. doi:10.1016/j.msard.2023.104545
11. Celik NG, Karabulut AK, Fazliogullari Z, Gumus H, Cebeci H, Dogan NU. Relationship between cervical spinal cord morphometry and clinical disability in patients with multiple sclerosis. *Rev Assoc Med Bras (1992)*. 2023;69(12):e20230949. doi:10.1590/1806-9282.20230949
12. Sechi E, Keegan BM, Kaufmann TJ, Kantarci OH, Weinshenker BG, Flanagan EP. Unilateral motor progression in MS: association with a critical corticospinal tract lesion. *Neurology*. 2019;93(7):e628-e634. doi:10.1212/WNL.0000000000007944
13. Breckwoldt MO, Gradl J, Hahnel S, et al. Increasing the sensitivity of MRI for the detection of multiple sclerosis lesions by long axial coverage of the spinal cord: a prospective study in 119 patients. *J Neurol*. 2017;264(2):341-349. doi:10.1007/s00415-016-8353-3
14. Ozturk A, Aygun N, Smith SA, Caffo B, Calabresi PA, Reich DS. Axial 3D gradient-echo imaging for improved multiple sclerosis lesion detection in the cervical spinal cord at 3T. *Neuroradiology*. 2013;55(4):431-439. doi:10.1007/s00234-012-1118-5
15. Galler S, Stellmann JP, Young KL, et al. Improved lesion detection by using axial T2-weighted MRI with full spinal cord coverage in multiple sclerosis. *AJNR Am J Neuroradiol*. 2016;37(5):963-969. doi:10.3174/ajnr.A4638
16. Wattjes MP, Ciccarelli O, Reich DS, et al. 2021 MAGNIMS-CMSC-NAIMS consensus recommendations on the use of MRI in patients with multiple sclerosis. *Lancet Neurol*. 2021;20(8):653-670. doi:10.1016/S1474-4422(21)00095-8
17. Dula AN, Pawate S, Dortch RD, et al. Magnetic resonance imaging of the cervical spinal cord in multiple sclerosis at 7T. *Mult Scler*. 2016;22(3):320-328. doi:10.1177/1352458515591070
18. Louapre C, Treaba CA, Barletta V, Mainero C. Ultra-high field 7T imaging in multiple sclerosis. *Curr Opin Neurol*. 2020;33(4):422-429. doi:10.1097/WCO.0000000000000839
19. Bergers E, Bot JC, van der Valk P, et al. Diffuse signal abnormalities in the spinal cord in multiple sclerosis: direct postmortem in situ magnetic resonance imaging correlated with in vitro high-resolution magnetic resonance imaging and histopathology. *Ann Neurol*. 2002;51(5):652-656. doi:10.1002/ana.10170
20. Bot JC, Blezer EL, Kamphorst W, et al. The spinal cord in multiple sclerosis: relationship of high-spatial-resolution quantitative MR imaging findings to histopathologic results. *Radiology*. 2004;233(2):531-540. doi:10.1148/radiol.2332031572
21. Gilmore CP, Geurts JJ, Evangelou N, et al. Spinal cord grey matter lesions in multiple sclerosis detected by post-mortem high field MR imaging. *Mult Scler*. 2009;15(2):180-188. doi:10.1177/1352458508096876
22. Nijeholt GJ, Bergers E, Kamphorst W, et al. Post-mortem high-resolution MRI of the spinal cord in multiple sclerosis: a correlative study with conventional MRI, histopathology and clinical phenotype. *Brain*. 2001;124(pt 1):154-166. doi:10.1093/brain/124.1.154
23. Gilmore CP, DeLuca GC, Bo L, et al. Spinal cord neuronal pathology in multiple sclerosis. *Brain Pathol*. 2009;19(4):642-649. doi:10.1111/j.1750-3639.2008.00228.x
24. Mottershead JP, Schmierer K, Clemence M, et al. High field MRI correlates of myelin content and axonal density in multiple sclerosis--a post-mortem study of the spinal cord. *J Neurol*. 2003;250(11):1293-1301. doi:10.1007/s00415-003-0192-3
25. Petrova N, Carassiti D, Altmann DR, Baker D, Schmierer K. Axonal loss in the multiple sclerosis spinal cord revisited. *Brain Pathol*. 2018;28(3):334-348. doi:10.1111/bpa.12516
26. DeLuca GC, Ebers GC, Esiri MM. Axonal loss in multiple sclerosis: a pathological survey of the corticospinal and sensory tracts. *Brain*. 2004;127(Pt 5):1009-1018. doi:10.1093/brain/awh118
27. Dutta R, Mahajan KR, Nakamura K, et al. Comprehensive autopsy program for individuals with multiple sclerosis. *J Vis Exp*. 2019;149:e59511. doi:10.3791/59511
28. Fisher E, Chang A, Fox RJ, et al. Imaging correlates of axonal swelling in chronic multiple sclerosis brains. *Ann Neurol*. 2007;62(3):219-228. doi:10.1002/ana.21113
29. *Statistical Parametric Mapping (SPM)*. fil.ion.ucl.ac.uk/spm/
30. Smith SM, Jenkinson M, Woolrich MW, et al. Advances in functional and structural MR image analysis and implementation as FSL. *Neuroimage*. 2004;23(suppl 1):S208-S219. doi:10.1016/j.neuroimage.2004.07.051
31. Bo L, Mork S, Kong PA, Nyland H, Pardo CA, Trapp BD. Detection of MHC class II-antigens on macrophages and microglia, but not on astrocytes and endothelia in active multiple sclerosis lesions. *J Neuroimmunol*. 1994;51(2):135-146. doi:10.1016/0165-5728(94)90075-2
32. Schindelin J, Arganda-Carreras I, Frise E, et al. Fiji: an open-source platform for biological-image analysis. *Nat Methods*. 2012;9(7):676-682. doi:10.1038/nmeth.2019
33. *R: A Language and Environment for Statistical Computing [Computer Program]*. R Foundation for Statistical Computing, 2020.
34. *Neuroimaging Tools and Resources Collaboratory (NITRC)*. nitrc.org/projects/mricrogl
35. Lefeuvre JA, Guy JR, Luciano NJ, et al. The spectrum of spinal cord lesions in a primate model of multiple sclerosis. *Mult Scler*. 2020;26(3):284-293. doi:10.1177/1352458518822408
36. Schading S, David G, Max Emmenegger T, et al. Dynamics of progressive degeneration of major spinal pathways following spinal cord injury: a longitudinal study. *Neuroimage Clin*. 2023;37:103339. doi:10.1016/j.nicl.2023.103339
37. Davies AL, Desai RA, Bloomfield PS, et al. Neurological deficits caused by tissue hypoxia in neuroinflammatory disease. *Ann Neurol*. 2013;74(6):815-825. doi:10.1002/ana.24006
38. Desai RA, Davies AL, Tachrount M, et al. Cause and prevention of demyelination in a model multiple sclerosis lesion. *Ann Neurol*. 2016;79(4):591-604. doi:10.1002/ana.24607
39. Peters S, Neves FB, Huhndorf M, et al. Detection of spinal cord multiple sclerosis lesions using a 3D-PSIR sequence at 1.5 T. *Clin Neuroradiol*. 2024;34(2):403-410. doi:10.1007/s00062-023-01376-x
40. Bateman GA, Bateman AR. The dilated veins surrounding the cord in multiple sclerosis suggest elevated pressure and obstruction of the glymphatic system. *Neuroimage*. 2024;286:120517. doi:10.1016/j.neuroimage.2024.120517
41. Ruggieri S, Prosperini L, Petracca M, et al. The added value of spinal cord lesions to disability accrual in multiple sclerosis. *J Neurol*. 2023;270(10):4995-5003. doi:10.1007/s00415-023-11829-5
42. Lorefice L, Piras C, Sechi V, Barracciu MA, Cocco E, Fenu G. Spinal cord MRI activity in multiple sclerosis: predictive value for relapses and impact on treatment decisions. *J Neurol Sci*. 2024;462:123057. doi:10.1016/j.jns.2024.123057

43. Karimian-Jazi K, Neuberger U, Schregel K, et al. Diagnostic value of gadolinium contrast administration for spinal cord magnetic resonance imaging in multiple sclerosis patients and correlative markers of lesion enhancement. *Mult Scler J Exp Transl Clin*. 2021;7(4):20552173211047978. doi:10.1177/20552173211047978
44. Tsagkas C, Horvath-Huck A, Haas T, et al. Fully automatic method for reliable spinal cord compartment segmentation in multiple sclerosis. *AJNR Am J Neuroradiol*. 2023;44(2):218-227. doi:10.3174/ajnr.A7756
45. Wenzel N, Wittayer M, Weber CE, Platten M, Gass A, Eisele P. Multiple sclerosis iron rim lesions are linked to impaired cervical spinal cord integrity using the T1/T2-weighted ratio. *J Neuroimaging*. 2023;33(2):240-246. doi:10.1111/jon.13076
46. Clarke MA, Witt AA, Robison RK, et al. Cervical spinal cord susceptibility-weighted MRI at 7T: application to multiple sclerosis. *Neuroimage*. 2023;284:120460. doi:10.1016/j.neuroimage.2023.120460
47. van der Poel M, Ulas T, Mizee MR, et al. Transcriptional profiling of human microglia reveals grey-white matter heterogeneity and multiple sclerosis-associated changes. *Nat Commun*. 2019;10(1):1139. doi:10.1038/s41467-019-08976-7
48. Lieury A, Chanal M, Androdias G, et al. Tissue remodeling in periplaque regions of multiple sclerosis spinal cord lesions. *Glia*. 2014;62(10):1645-1658. doi:10.1002/glia.22705
49. Schirmer L, Antel JP, Bruck W, Stadelmann C. Axonal loss and neurofilament phosphorylation changes accompany lesion development and clinical progression in multiple sclerosis. *Brain Pathol*. 2011;21(4):428-440. doi:10.1111/j.1750-3639.2010.00466.x
50. Bjartmar C, Kidd G, Mork S, Rudick R, Trapp BD. Neurological disability correlates with spinal cord axonal loss and reduced N-acetyl aspartate in chronic multiple sclerosis patients. *Ann Neurol*. 2000;48(6):893-901. doi:10.1002/1531-8249(200012)48:6<893::aid-ana10>3.3.co;2-2